Electrohydrodynamics and dielectrophoresis in microsystems: scaling laws

A Castellanos[1], **A Ramos**[1], **A González**[1,2], **N G Green**[3] and **H Morgan**[3,4]

[1] Dpto. Electrónica y Electromagnetismo, Facultad de Física, Universidad de Sevilla, Reina Mercedes s/n, 41012 Sevilla, Spain
[2] Dpto. de Física Aplicada III, E.S.I. Universidad de Sevilla, Camino de los Descubrimientos s/n 41092 Sevilla, Spain
[3] Bioelectronics Research Centre, Dept. Electronics and Electrical Engineering, University of Glasgow, Oakfield Avenue, Glasgow G12 8LT, UK

Abstract

The movement and behaviour of particles suspended in aqueous solutions subjected to non-uniform ac electric fields is examined. The ac electric fields induce movement of polarizable particles, a phenomenon known as dielectrophoresis. The high strength electric fields that are often used in separation systems can give rise to fluid motion, which in turn results in a viscous drag on the particle. The electric field generates heat, leading to volume forces in the liquid. Gradients in conductivity and permittivity give rise to electrothermal forces and gradients in mass density to buoyancy. In addition, non-uniform ac electric fields produce forces on the induced charges in the diffuse double layer on the electrodes. This causes a steady fluid motion termed ac electro-osmosis. The effects of Brownian motion are also discussed in this context. The orders of magnitude of the various forces experienced by a particle in a model microelectrode system are estimated. The results are discussed in relation to experiments and the relative influence of each type of force is described.

1. Introduction

The application of ac electrokinetic forces to control and manipulate isolated particles in suspension using microelectrode structures is a well-established technique [1]. In particular, the dielectrophoretic manipulation of sub-micron bioparticles such as viruses, cells and DNA is now possible. As the size of the particle is reduced, so the effects of Brownian motion become greater. Therefore, to enable the dielectrophoretic manipulation of sub-micron particles using realistic voltages the characteristic dimensions of the system must be reduced to increase the electric field. However, a high strength electric field also produces a force on the suspending electrolyte, setting it into motion. Indeed, this motion may be a far greater limiting factor than Brownian motion.

Owing to the intensity of the electric fields required to move sub-micrometre particles, Joule heating can be a problem, often giving rise to electrical forces induced by the variation in the conductivity and permittivity of the suspending medium (electrothermal forces) [2–4]. In certain circumstances, Joule heating may be great enough to cause buoyancy forces. In addition to Joule heating, the geometry of the electrodes used to generate dielectrophoretic forces produces a tangential electric field at the electrode–electrolyte double layer. This induces steady motion of the liquid, a flow termed ac electro-osmosis because of its similarity to electro-osmosis in a dc field [5–8]. It should be emphasized that the ac electro-osmotic flow observed over microelectrodes differs from ac electro-osmosis observed in capillaries [9]. In the latter case, the electric field is uniform along the capillary but time-varying. The diffuse double layer charge is fixed and the fluid motion is oscillatory. However, in the former case both

the electric field and the double layer charge are time-varying and give rise to a steady fluid motion.

Based on these mechanisms, the magnitude and direction of the surface and volume forces acting on the liquid can be predicted analytically or, alternatively, using numerical simulations. This means that it should be possible to design and develop microelectrode structures that can translate experimental and theoretical understanding into a given specification. However, the precise design of a complicated microelectrode structure would require extensive numerical calculations. The aim of this paper is to develop a general framework that outlines the basic constraints of a system, thus reducing the need for intensive computation. A first step in this process is prior knowledge of how the forces on the particle scale with the size of the system, the shape of the electrodes, the particle diameter, the magnitude and frequency of the applied ac electric field, and the conductivity of the suspending solution.

In this paper, we present an analysis of particle dynamics and a summary of the type of fluid flow observed in a simplified system consisting of two co-planar parallel strip electrodes. Previously published data are reviewed and new analyses performed to determine a general understanding of the scaling laws governing this simple system. Within limits, these results can be generalized to more complicated microelectrode shapes, bearing in mind that different regions of the system may have different characteristic length scales.

Bioparticles have sizes that range from $0.1\,\mu$m up to $10\,\mu$m, e.g. viruses (0.01–$0.1\,\mu$m), bacteria (0.5–$5\,\mu$m), or plant or animal cells (5–$15\,\mu$m). They are usually suspended in an aqueous saline solution with a conductivity that ranges between 10^{-4} and $1\,\mathrm{S\,m^{-1}}$. Typical system lengths of the microelectrodes (interelectrode gaps) used in the dielectrophoretic manipulation of bioparticles vary from 1 to $500\,\mu$m. The signals applied to these electrodes can be up to 20 V giving rise to electric fields that can be as high as $5 \times 10^6\,\mathrm{V\,m^{-1}}$. The applied signals have frequencies in the range 10^2–10^8 Hz.

As stated previously, measurement and analysis of flow has been performed using a simple electrode design consisting of two coplanar rectangular electrodes fabricated on a glass substrate. The electrodes are 2 mm long and $500\,\mu$m wide, with parallel edges separated by a $25\,\mu$m gap [8, 10]. A schematic diagram of the system is shown in figure 1, together with a simplified idealization of the system. Because the gap is small compared to the length and width of the electrodes the system can be considered to be two-dimensional [7, 11], so that the analysis is restricted to the two-dimensional cross-section shown in figure 1. Such a simplified system can give useful information on the relative magnitudes of the different forces generated, together with the regions where certain approximations are valid. Extending the general results obtained for the two-dimensional planar electrode to other geometries must be done with care. For example, figure 2 shows two different electrode arrays: a hyperbolic polynomial electrode and a castellated electrode. In this case, several different length scales act at the same time.

The first part of the paper is an analysis of the motion of particles caused by gravity, dielectrophoresis (DEP) and Brownian motion. The mechanical, electrical and thermal
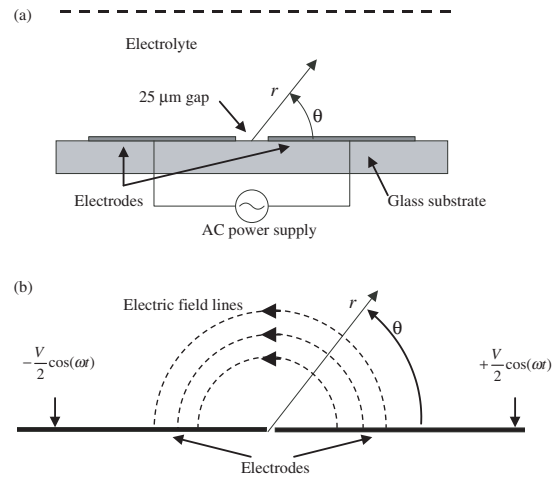

Figure 1. (*a*) Schematic diagram of the electrodes used to move particles and fluids. (*b*) Simplified ideal system showing the electrical field lines.

equations that govern liquid motion in these microelectrode structures are then formulated. The volume and surface forces acting on the system are given, emphasizing how these forces scale with system parameters. Finally, the relative importance of the drag force (which comes from electrohydrodynamic flow) is discussed and compared with Brownian motion, DEP and gravitational forces.

2. Particle motion

2.1. Stokes force

For simplicity, consider the particles to be spherical. Assuming that the Stokes drag is valid, the movement of a particle in a fluid influenced by a force $\boldsymbol{F}$, is governed by

$$m\frac{\mathrm{d}\boldsymbol{u}}{\mathrm{d}t} = -\gamma(\boldsymbol{u}-\boldsymbol{v}) + \boldsymbol{F} \tag{1}$$

where m is the particle mass, $\boldsymbol{u}$ the particle velocity and $\boldsymbol{v}$ the fluid velocity, $-\gamma(\boldsymbol{u}-\boldsymbol{v})$ is the drag force with γ the friction factor of the particle in the fluid. For a spherical particle $\gamma = 6\pi\eta a$, where a is the particle radius and η is the viscosity of the medium. Under the action of a constant force $\boldsymbol{F}$ and fluid velocity $\boldsymbol{v}$, the particle velocity is

$$\boldsymbol{u} = \left(\boldsymbol{u}_0 - \boldsymbol{v} - \frac{\boldsymbol{F}}{\gamma}\right)\mathrm{e}^{-(\gamma/m)t} + \boldsymbol{v} + \frac{\boldsymbol{F}}{\gamma} \tag{2}$$

where $\boldsymbol{u}_0$ is the initial velocity of the particle. The characteristic time of acceleration, $\tau_\mathrm{a} = m/\gamma$, is usually much smaller than the typical time of observation (~ 1 s). For a spherical particle of mass density ρ_p, $\tau_\mathrm{a} = (\frac{2}{9})(\rho_\mathrm{p}a^2/\eta)$, which is smaller than 10^{-6} s for cells and sub-micrometre particles. Therefore, the particle can be considered to move at its terminal velocity, given by

$$\boldsymbol{u} = \boldsymbol{v} + \frac{\boldsymbol{F}}{\gamma} \tag{3}$$

This means that any measurement of particle velocity is a direct measure of the fluid velocity, $\boldsymbol{v}$, plus the velocity induced by the force acting on the particle, $\boldsymbol{F}/\gamma$. In general, the acceleration process is much more complicated than described by the simple
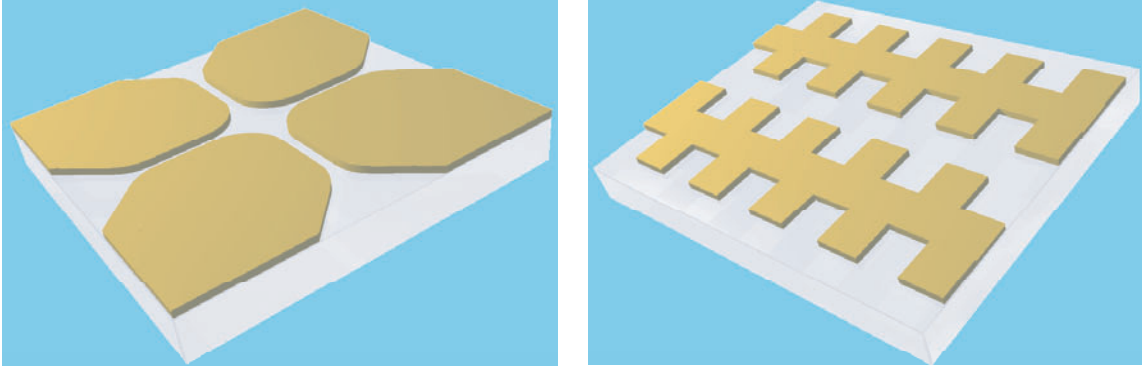
2585

Figure 2. Diagram of a hyperbolic polynomial electrode (left) and a castellated electrode (right).

exponential solution, and the acceleration of the fluid and diffusion of vorticity must also be considered [12]. However, the fact that the particle moves at its terminal velocity for times much greater than $\rho_p a^2/\eta$ is still valid.

2.2. Gravity

The main external influence on a particle suspended in a fluid is gravity. For a particle of mass density ρ_p in a fluid of density ρ_m the gravitational force is given by

$$F_g = \upsilon(\rho_p - \rho_m)g \qquad (4)$$

where g is the acceleration due to gravity and υ is the volume of the particle. The magnitude of the velocity of a spherical particle in a gravitational field is

$$u_g = \frac{\upsilon|\rho_p - \rho_m|g}{f} = \frac{2}{9}\frac{a^2|\rho_p - \rho_m|g}{\eta} \qquad (5)$$

To a first-order approximation, assume $|\rho_p - \rho_m|$ is of the order of ρ_m; then, the magnitude of the gravitational velocity can be estimated to be

$$u_g \sim 0.2\frac{a^2\rho_m g}{\eta} \qquad (6)$$

In this expression, the factor 0.2 may be smaller since many particles have densities that are close to that of water.

2.3. Dielectrophoresis

Particles in electric fields are subjected to electrophoretic and dielectrophoretic forces. In the thin double layer approximation, the velocity induced by the former force is given by the Smoluchowsky formula, $u = \varepsilon\zeta E/\eta$, where ε and η are, respectively, the electrical permittivity and dynamic viscosity of water, and ζ is the zeta potential of the particle. In ac electric fields, the particle displacement is oscillatory with a maximum amplitude given by $\Delta x = u/\omega$, which for sufficiently high frequencies can be neglected. For example, for a field amplitude of 10^5 V m^{-1}, a frequency of 1 kHz and a zeta potential of 50 mV, the displacement $\Delta x \sim 0.5\,\mu$m. In fact this is a gross overestimation because particle inertia would lead to a smaller net displacement that decreases with increasing frequency, proportional to ω^{-2}. In contrast, the DEP force has a non-zero time average and leads to net particle displacement.

The dielectrophoretic force arises from the interaction of a non-uniform electric field and the dipole induced in the particle. For linear, isotropic dielectrics, the relationship between the dipole moment phasor p of a spherical particle and the electric field phasor E is given by $p(\omega) = \upsilon\alpha(\omega)E$, where α is the effective polarizability of the particle and ω is the angular frequency of the electric field. The time-averaged force on the particle is given by [13]

$$\langle F_{DEP} \rangle = \tfrac{1}{2}\text{Re}[(p \cdot \nabla)E^*] = \tfrac{1}{4}\upsilon\text{Re}[\alpha]\nabla|E|^2$$
$$- \tfrac{1}{2}\upsilon\text{Im}[\alpha](\nabla \times (\text{Re}[E] \times \text{Im}[E])) \qquad (7)$$

where $*$ indicates complex conjugation, Re$[A]$ and Im$[A]$ the real and imaginary parts of A and $|E|^2 = E \cdot E^*$. For the second equality, E has been considered to be solenoidal, i.e. $\nabla \cdot E = 0$. The first term on the right-hand side is non-zero if there is a spatially varying field magnitude, giving rise to DEP. The second term is non-zero if there is a spatially varying phase, as in the case of travelling wave dielectrophoresis (twDEP). If the particle polarizes by the Maxwell–Wagner mechanism, and considering only the dipole force, the DEP-induced velocity of a spherical particle is

$$u_{DEP} = \frac{\upsilon\text{Re}[\alpha]}{4\gamma}\nabla|E|^2 = \frac{a^2\varepsilon}{6\eta}\text{Re}\left[\frac{\tilde{\varepsilon}_p - \tilde{\varepsilon}}{\tilde{\varepsilon}_p + 2\tilde{\varepsilon}}\right]\nabla|E|^2 \qquad (8)$$

Here $\tilde{\varepsilon}$ indicates a complex permittivity, $\tilde{\varepsilon} = \varepsilon - i\sigma/\omega$, where ε is the permittivity and σ is the conductivity. The expression in brackets is referred to as the Clausius–Mossotti factor and describes the frequency variation of the dielectrophoretic mobility and force. This factor varies between $+1$ and $-\tfrac{1}{2}$; the particle moves towards (positive DEP) or away from (negative DEP) regions of high field strength, depending on frequency.

For the sake of simplified analysis, the electric field lines between the electrodes can be considered semi-circular as shown in figure 1(b); in this case, the electric field is given by $E = V/\pi r u_\theta$, where V is the amplitude of the applied voltage and r is the distance to the centre of the gap. This expression is the exact solution for the field when the electrodes are semi-infinite with an infinitely small gap.

Assuming a Clausius–Mossotti factor of 1 and an electric field given by $E = V/\pi r$, the magnitude of the dielectrophoretic velocity of a particle in this system, at a distance r from the centre, is

$$u_{DEP} \approx 0.03\frac{a^2\varepsilon}{\eta}\frac{V^2}{r^3} \qquad (9)$$

2.4. Brownian motion

Thermal effects also influence colloidal particles. The force and velocity associated with Brownian motion have zero average; however, the random displacement of the particle follows a Gaussian profile with a root-mean-square displacement (in one dimension) given by

$$\Delta x = \sqrt{2Dt} = \sqrt{\frac{k_B T}{3\pi a\eta}t} \qquad (10)$$

where k_B is Boltzman's constant, T is the absolute temperature and t is the period of observation. To move an isolated particle in a deterministic manner during this period, the displacement due to the deterministic force should be greater than that due to the random (Brownian) motion. This consideration is meaningful only for single isolated particles. For a collection of particles, diffusion of the ensemble must be considered.

2.5. Particle displacements

The influence of these three forces, viz Brownian, gravitational and dielectrophoretic forces, on a single particle can be summarized with reference to figure 3. This shows a plot of the displacement of a particle during a time interval of 1 s as a function of particle radius. For the particular parameter set used to calculate this figure, it can be seen that the displacement due to Brownian motion is greater than that due to DEP at 5 V for a particle of less than 0.2 μm radius. Also, for this parameter set, the gravitational motion is less important than DEP for any particle size since both scale as a^2. Note that the particle should be much smaller than the characteristic length of the system, in this case $r = 25\,\mu$m. The deterministic manipulation of isolated particles smaller than 0.2 μm can be achieved if the magnitude of the applied voltage is increased, or the characteristic length of the system r is reduced. In this context, the figure shows the effect of increasing the voltage by a factor of three, which increases the displacement due to DEP by one order of magnitude. Although the figure shows that it should be relatively easy to move small particles simply by increasing the electric field, this naïve assumption presumes that no other forces appear in the system. However, in many situations, the electric field can produce a body force on the
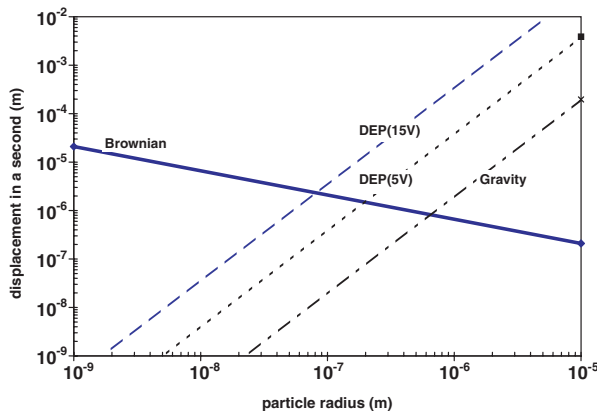

Figure 3. Particle displacement in 1 s versus particle radius for a particle of mass density 1050 kg m^{-3}. The characteristic length used in this figure is $r = 25\,\mu$m.

fluid setting it into motion resulting in the movement of a particle through the Stokes drag.

3. Electrohydrodynamics

3.1. Electrical equations

The electromagnetic field in the bulk is governed by Maxwell's equations. For microelectrode structures magnetic effects can be neglected when compared with the electric field since the energy stored in the magnetic field is much smaller than the electrical energy. The condition for this is

$$\frac{W_M}{W_E} = \frac{(1/2)\mu H^2}{(1/2)\varepsilon E^2} \ll 1 \qquad (11)$$

where μ is the magnetic permeability of the medium. The magnetic field is produced by both conduction and displacement currents. If conduction currents dominate, the magnetic field intensity can be estimated from Ampere's law as $H \sim \sigma E l$, with l a characteristic length of the system. For saline solutions with $\sigma < 0.1\,\mathrm{S\,m^{-1}}$ and a typical system length of $l < 1$ mm,

$$\frac{W_M}{W_E} \sim \frac{\mu\sigma^2 l^2}{\varepsilon} < 10^{-5} \qquad (12)$$

If displacement currents dominate, an estimate of the magnetic field intensity can be made from $H \sim \omega\varepsilon E l$. For frequencies smaller than 10 MHz and system length $l < 1$ mm,

$$\frac{W_M}{W_E} \sim \mu\varepsilon\omega^2 l^2 < 3 \times 10^{-6} \qquad (13)$$

Under these conditions the electromagnetic equations reduce to those in the quasi-electrostatic limit [14]:

$$\nabla \cdot (\varepsilon \boldsymbol{E}) = \rho_q \qquad (14)$$

$$\nabla \times \boldsymbol{E} = 0 \qquad (15)$$

$$\nabla \cdot \boldsymbol{j} + \frac{\partial\rho_q}{\partial t} = 0 \qquad (16)$$

where ρ_q is the volume charge density. In the bulk electrolyte, the electric current $\boldsymbol{j}$ is given by Ohm's law, $\boldsymbol{j} = \sigma\boldsymbol{E}$. For a binary symmetrical electrolyte the current density is given by

$$\boldsymbol{j} = e(n_+ + n_-)\mu_e\boldsymbol{E} - eD\nabla(n_+ - n_-) + e(n_+ - n_-)\boldsymbol{v} \qquad (17)$$

with e the absolute value of electronic charge, μ_e, D, n_+ and n_-, the mobility, diffusion coefficient and number densities of positive and negative ions. Gauss' law suggests that saline solutions are electrically neutral on the micrometre length scale [15]. In effect, the relative difference in ion number densities is given by the ratio

$$\Lambda = \frac{n_+ - n_-}{n_0} = \frac{\nabla \cdot (\varepsilon \boldsymbol{E})}{en_0} \sim \frac{\varepsilon E}{en_0 l} \qquad (18)$$

with n_0 the unperturbed ion density. For values of $E \sim 10^5\,\mathrm{V\,m^{-1}}$, $n_0 \sim 10^{23}\,\mathrm{m^{-3}}$ and typical system length $l \sim 10\,\mu$m then $\Lambda \sim 4 \times 10^{-4}$ and the liquid bulk is quasi-electroneutral. Now, comparing the diffusion to the electric drift, we obtain

$$\frac{|eD\nabla(n_+ - n_-)|}{e(n_+ + n_-)\mu_e E} \sim \frac{D\varepsilon E/l^2}{e2n_0\mu_e E} = \left(\frac{\lambda_D}{l}\right)^2 \qquad (19)$$

where $\lambda_{\mathrm{D}} = \sqrt{\varepsilon D/2en_0\mu_{\mathrm{e}}}$ is the Debye length, which is of the order of several nanometres, much smaller than the typical system length.

Defining $\sigma = 2en_0\mu_{\mathrm{e}}$, we now compare the conduction current, $\sigma\boldsymbol{E}$, to the convection current, $\rho_q\boldsymbol{v}$ in saline solutions. Taking typical values $\sigma \sim 10^{-3}\,\mathrm{S\,m^{-1}}$, $l \sim 10\,\mu\mathrm{m}$, $v \sim 100\,\mu\mathrm{m\,s^{-1}}$ gives

$$\frac{|\nabla \cdot (\varepsilon\boldsymbol{E})\,\boldsymbol{v}|}{|\sigma\boldsymbol{E}|} \sim \frac{\varepsilon/\sigma}{l/v} \sim 7 \times 10^{-6} \tag{20}$$

The combination of parameters, $\varepsilon v/l\sigma$, is called the electrical Reynolds number [16], and since it is very small the electrical equations are decoupled from the mechanical equations. Therefore, neglecting the convective term, and assuming that σ and ε are independent of time, equations (14) and (16) can be combined (for an ac field of frequency ω) as

$$\nabla \cdot ((\sigma + \mathrm{i}\omega\varepsilon)\boldsymbol{E}) = 0 \tag{21}$$

where $\boldsymbol{E}$ is now a complex vector.

In many cases, the gradients in permittivity and conductivity are small [3, 11], so that the electric field can be expanded to give $\boldsymbol{E} = \boldsymbol{E}_0 + \boldsymbol{E}_1$, $(|\boldsymbol{E}_1| \ll |\boldsymbol{E}_0|)$, where the electric fields satisfy the equations

$$\nabla \cdot \boldsymbol{E}_0 = 0 \tag{22}$$

$$\nabla \cdot \boldsymbol{E}_1 + \left(\frac{\nabla\sigma + \mathrm{i}\omega\nabla\varepsilon}{\sigma + \mathrm{i}\omega\varepsilon}\right) \cdot \boldsymbol{E}_0 = 0 \tag{23}$$

The charge density of each order can be approximated to

$$\rho_0 = \varepsilon\nabla \cdot \boldsymbol{E}_0 = 0 \tag{24}$$

$$\rho_1 = \varepsilon\nabla \cdot \boldsymbol{E}_1 + \nabla\varepsilon \cdot \boldsymbol{E}_0 = \left(\frac{\sigma\nabla\varepsilon - \varepsilon\nabla\sigma}{\sigma + \mathrm{i}\omega\varepsilon}\right) \cdot \boldsymbol{E}_0 \tag{25}$$

In our analysis, only the zero-order field $\boldsymbol{E}_0$ is required, which is obtained from the solution of Laplace's equation

$$\nabla^2\phi_0 = 0 \tag{26}$$

3.2. Mechanical equations

Liquid motion is governed by the Navier–Stokes equations for an incompressible fluid

$$\nabla \cdot \boldsymbol{v} = 0 \tag{27}$$

$$\rho_{\mathrm{m}}\left(\frac{\partial\boldsymbol{v}}{\partial t} + (\boldsymbol{v} \cdot \nabla)\boldsymbol{v}\right) = -\nabla p + \eta\nabla^2\boldsymbol{v} + \boldsymbol{f}_{\mathrm{E}} + \rho_{\mathrm{m}}\boldsymbol{g} \tag{28}$$

where $\boldsymbol{f}_{\mathrm{E}}$ represents the electrical forces, and $\rho_{\mathrm{m}}\boldsymbol{g}$, the action of gravity.

For microsystems the Reynolds number is usually very small; typical velocity $v < 100\,\mu\mathrm{m\,s^{-1}}$, and dimension $l < 100\,\mu\mathrm{m}$ and

$$\frac{|\rho_{\mathrm{m}}(\boldsymbol{v} \cdot \nabla)\boldsymbol{v}|}{|\eta\nabla^2\boldsymbol{v}|} \sim \mathrm{Re} = \frac{\rho_{\mathrm{m}}vl}{\eta} \leqslant 10^{-2} \tag{29}$$

Therefore, the convective term in the Navier–Stokes can be neglected.

After application of the electric field, a stationary state is reached in a time of the order of $t = \rho_{\mathrm{m}}l^2/\eta$, which is usually smaller than 0.01 s. Since the electrical force is oscillatory with a non-zero time average, the steady-state liquid motion can have both a non-zero time-averaged component and an oscillating one. We are interested in the time-averaged component, the one that is easily seen in the experiments. The equation for the average velocity can then be written as

$$0 = -\nabla p + \eta\nabla^2\boldsymbol{v} + \langle\boldsymbol{f}_{\mathrm{E}}\rangle + \Delta\rho_{\mathrm{m}}\boldsymbol{g} \tag{30}$$

Here, since the mass density of the fluid is almost homogeneous, the Boussineq approximation has been applied, i.e. changes in density are neglected except for the buoyancy force [17]. As stated by this equation, the fluid motion is caused by the combined action of gravity and electrical forces. The latter is given by [18]

$$\boldsymbol{f}_{\mathrm{E}} = \rho_q\boldsymbol{E} - \frac{1}{2}|\boldsymbol{E}|^2\nabla\varepsilon + \nabla\left(\frac{1}{2}\rho_{\mathrm{m}}\left(\frac{\partial\varepsilon}{\partial\rho_{\mathrm{m}}}\right)_T E^2\right) \tag{31}$$

For incompressible fluids, the third term in this equation, the electrostriction, can be incorporated into the pressure [18] and omitted from the calculations. The first term, the Coulomb force, and the second term, the dielectric force, depend on the presence of gradients in the conductivity and permittivity. For an applied ac voltage, the electrical force has a non-zero time average given by

$$\langle\boldsymbol{f}_{\mathrm{E}}\rangle = \tfrac{1}{2}\mathrm{Re}(\rho_q\boldsymbol{E}^*) - \tfrac{1}{4}\boldsymbol{E} \cdot \boldsymbol{E}^*\nabla\varepsilon \tag{32}$$

where the charge and field on the right-hand side are the complex amplitudes. Substituting for the charge from equations (24) and (25), and provided the gradients are small, gives [3, 11]

$$\langle\boldsymbol{f}_{\mathrm{E}}\rangle = \frac{1}{2}\mathrm{Re}\left(\left(\left(\frac{\sigma\nabla\varepsilon - \varepsilon\nabla\sigma}{\sigma + \mathrm{i}\omega\varepsilon}\right) \cdot \boldsymbol{E}_0\right)\boldsymbol{E}_0^*\right) - \frac{1}{4}\boldsymbol{E}_0 \cdot \boldsymbol{E}_0^*\nabla\varepsilon \tag{33}$$

This expression for the electrical forces is clearly frequency dependent. If ω is much greater than σ/ε, the second term (the dielectric force) dominates. Likewise, if $\omega \ll \sigma/\varepsilon$, the first term, the Coulomb force, dominates because relative variations in conductivity ($\Delta\sigma/\sigma$) are usually much greater than relative variations in permittivity ($\Delta\varepsilon/\varepsilon$). This is the case for variations caused by gradients in temperature, where for electrolytes $(1/\sigma)(\partial\sigma/\partial T) \approx 0.02\,\mathrm{K^{-1}}$ and $(1/\varepsilon)(\partial\varepsilon/\partial T) \approx -0.004\,\mathrm{K^{-1}}$.

Both electrical and gravitational forces are present when the liquid is inhomogeneous. In the following analysis, gradients in permittivity, conductivity and mass density are assumed to arise from the temperature gradients present in the fluid.

3.3. Energy equation

Together with the electrical and mechanical equations, the equation for the internal energy is required, which can be related to the temperature distribution through [3]

$$\rho_{\mathrm{m}}c_p\left(\frac{\partial T}{\partial t} + (\boldsymbol{v} \cdot \nabla)T\right) = k\nabla^2 T + \sigma E^2 \tag{34}$$

where c_p is the specific heat (at constant pressure) and k is the thermal conductivity of the fluid. After the application of the electric field, the temperature field rapidly reaches a stationary state that has both a time-independent component and an oscillating one, in a manner similar to the velocity field. The effect of the oscillating component on the fluid dynamics is negligible for frequencies higher than 1 kHz [3]. The steady-state is reached after a time of the order of $t = \rho_\mathrm{m} c_p l^2/k$, which is usually smaller than 0.1 s.

For microsystems, heat convection is small compared to heat diffusion, as demonstrated by the small value of the Peclet number, which, typically ($v < 100\,\mu\mathrm{m\,s^{-1}}$ and $l < 100\,\mu\mathrm{m}$), is

$$\frac{|\rho_\mathrm{m} c_p (\boldsymbol{v} \cdot \nabla) T|}{|k\nabla^2 T|} \sim \mathrm{Pe} = \frac{\rho_\mathrm{m} c_p v l}{k} < 7 \times 10^{-2} \qquad (35)$$

Therefore, the temperature equation reduces to Poisson's equation, with Joule heating as the energy source

$$k\nabla^2 T = -\sigma \langle E^2 \rangle \qquad (36)$$

4. Boundary conditions

A summary of the electrohydrodynamic equations are given in table 1. In order to solve the equations, appropriate boundary conditions have to be defined. The domain boundary is composed of several parts. The boundary conditions for the electrodes (which are fabricated on glass) are summarized in figure 4, where the lateral and upper boundaries can be considered rigid and assumed to be far from the region of interest.

4.1. Electric potential

The electric field is produced by electrodes connected to ac voltage sources. The electric potential at the surface of the electrodes, V is fixed by the source. However, this is not necessarily the most suitable boundary condition to describe the behaviour of the potential in the bulk electrolyte ϕ, since a double layer lies between the metallic surface and the bulk electrolyte [19]. The appropriate boundary condition is the charge conservation equation for the double layer: the current into an element of the double layer is equal to the increase in the stored charge. Since the typical system length is much greater than the double layer thickness, the thin double-layer approximation can be used. Under this approximation, the lateral currents along the double layer (either convection or conduction) are negligible by comparison with the normal current. The ratio between tangential and normal conduction currents is of the order of λ_D/l. The ratio between tangential convective and normal conduction currents is of the order of $q_\mathrm{s} v/\sigma E l \sim v\varepsilon/\sigma\lambda_\mathrm{D}$, where q_s is the surface charge density in the double layer. If the slip velocity is much smaller than, typically, $10\,\mathrm{cm\,s^{-1}}$, then this ratio is much smaller than unity. Therefore, the normal current into the double layer is equal to the increase in the stored charge. Essentially, the size of the double layer is so small that it does not enter into the problem space. The electrical behaviour of a perfectly polarizable double layer can be modelled theoretically as a distributed capacitor between the electrode and the bulk. The conservation of charge condition then becomes [7, 8]

$$\sigma \frac{\partial \phi}{\partial n} = \frac{\partial}{\partial t}(C(\phi - V)) \qquad (37)$$

where n represents the outer normal, C the capacitance per unit area and ϕ the electric potential just outside the double layer. A typical value of the specific double layer capacitance C is given by the ratio of the electrolyte permittivity to the Debye length, $C \sim \varepsilon/\lambda_\mathrm{D}$. Using complex amplitudes, the boundary condition for ϕ at the electrode is a mixed boundary condition:

$$\phi - \frac{\sigma}{\mathrm{i}\omega C} \frac{\partial \phi}{\partial n} = V \qquad (38)$$

More generally, the behaviour of the double layer can be modelled through an empirical impedance. The boundary condition for the potential then becomes

$$\phi - \frac{\sigma}{Y} \frac{\partial \phi}{\partial n} = V \qquad (39)$$

with Y the admittance per unit area of the double layer. For the sake of simplicity we will assume that the electrodes are perfectly polarizable, with $Y = \mathrm{i}\omega C$. For frequencies $\omega \gg \sigma/(lC) \sim (\sigma/\varepsilon)(\lambda_\mathrm{D}/l)$, the boundary condition for the electric potential at the electrodes reduces to a fixed value of potential.

In writing equation (37), it has been assumed that $\omega \ll \sigma/\varepsilon$ and the displacement current has not been taken into account. This can be neglected since at a frequency where the displacement current dominates ($\omega > \sigma/\varepsilon$), the potential ϕ just outside the double layer becomes equal to the applied potential V.

Table 1. Summary of electrohydrodynamic equations.

	Electrical equations
Gauss' law	$\nabla \cdot \boldsymbol{E}_0 = 0$
Faraday's law	$\nabla \times \boldsymbol{E}_0 = 0$
Average electrical volume force	$\langle \boldsymbol{f}_\mathrm{E} \rangle = \frac{1}{2}\mathrm{Re}\left(\left(\left(\frac{\sigma\nabla\varepsilon - \varepsilon\nabla\sigma}{\sigma + \mathrm{i}\omega\varepsilon}\right) \cdot \boldsymbol{E}_0\right)\boldsymbol{E}_0^*\right) - \frac{1}{4}\boldsymbol{E}_0 \cdot \boldsymbol{E}_0^*\nabla\varepsilon$
	Mechanical equations
Incompressibility	$\nabla \cdot \boldsymbol{v} = 0$
Stokes' equation	$0 = -\nabla p + \eta\nabla^2\boldsymbol{v} + \langle \boldsymbol{f}_\mathrm{E} \rangle + \rho\boldsymbol{g}$
	Energy equation
Temperature diffusion	$\nabla^2 T = -\dfrac{\sigma\langle E^2 \rangle}{k}$

For the gap between the electrodes, i.e. the glass/electrolyte interface, the boundary condition is given by the continuity of the total normal current density:

$$(\sigma_G + i\omega\varepsilon_G)\frac{\partial\phi_G}{\partial n} = (\sigma + i\omega\varepsilon)\frac{\partial\phi}{\partial n} \quad (40)$$

where the subscript G is used for the electrical properties of the glass. In most situations, the large difference between the conductivities and permittivities of the water and the glass allows this boundary condition to be simplified to

$$\frac{\partial\phi}{\partial n} = 0 \quad (41)$$

If the upper boundary is far enough from the electrodes, it can be considered to be at infinity and the electric field and potential tend to zero.

4.2. Velocity

In any of the rigid boundaries, the normal velocity vanishes. The tangential velocity, however, can be non-zero on the electrodes. This is due to the presence of the double layer at the electrolyte/electrode interface. The effect of the tangential ac field on the oscillating induced charges in the double layer can be modelled as surface stresses that produce a slip velocity given by a generalization of the Smoluchowsky formula. The time-averaged expression for the slip velocity is given by [7, 8]

$$v_{slip} = \frac{1}{2}\frac{\varepsilon}{\eta}\Lambda\text{Re}[(\Delta\phi)E_t^*] = -\frac{1}{4}\frac{\varepsilon}{\eta}\Lambda\frac{\partial}{\partial x}|\Delta\phi|^2 \quad (42)$$

where $\Delta\phi_{DL} = \phi - V$ represents the voltage drop across the double layer and E_t is the tangential field just outside the double layer. The parameter Λ is an empirical constant that accounts for the ratio of the voltage drop across the diffuse part of the double layer (where the stresse is) to the total voltage drop across the double layer. For an ideal capacitive double layer formed by a Stern or compact layer (including electrode oxide layers) and a diffuse layer, Λ is given by

$$\Lambda = \frac{C_S}{C_S + C_D} \quad (43)$$

where C_S and C_D are the capacitances per unit of area of the Stern and diffuse layers, respectively. For the glass boundary the effect of the double layer is negligible and the tangential velocity vanishes due to viscous friction [8]. The electrical and mechanical boundary conditions pertinent to the plane where the electrodes are located are summarized in figure 4.

4.3. Temperature

From the theoretical point of view, the boundary conditions for the temperature field are the usual ones of continuity of temperature and continuity of normal heat fluxes at boundaries. In devices with microelectrodes, the boundary conditions for the temperature field are given by the ambient surroundings, which can differ significantly from one experiment to another. For example, the electrodes might be thick and conduct heat easily, so that the electrodes can be considered to be at room temperature. Equally, they might be very thin, the heat passing
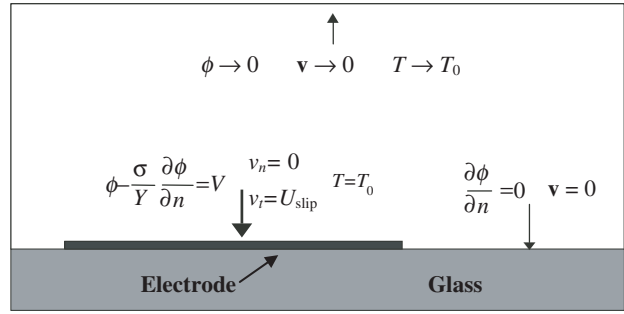
Figure 4. Electrical and mechanical boundary conditions on the plane of the electrodes.

through them as if they were transparent. For the calculations presented in this work, the electrodes are considered to be at room temperature. In addition, the upper and lateral boundaries will also be considered to be at room temperature, and positioned at a distance of the order of the total size of the system. The differences that occur between different extreme boundary conditions have been discussed in a previous paper [11].

5. Fluid flow

5.1. Joule-heating induced fluid flow

5.1.1. Electrothermal flow. Joule heating produces a temperature field that depends on the boundary conditions within a system. An order of magnitude estimate of the incremental temperature rise can be made by substituting for the electric field in equation (36) to give

$$\frac{k\Delta T}{l^2} \sim \frac{\sigma V^2}{2l^2} \quad \text{or} \quad \Delta T \sim \frac{\sigma V^2}{2k} \quad (44)$$

where V is the amplitude of the ac signal applied between electrodes. Since the temperature increment does not depend on the typical size of the system, reducing the system dimensions will lower the voltage required to produce a given electric field and as a result reduce the temperature increment. For the simplified ideal system of figure 1(*b*) and assuming that the electrodes are at constant temperature, the analytical solution [3] is

$$\Delta T = \frac{\sigma V^2}{2k}\left(\frac{\theta}{\pi} - \frac{\theta^2}{\pi^2}\right) \quad (45)$$

where θ is the angle measured from one electrode. This solution gives a maximum temperature increment of $\Delta T = \sigma V^2/8k$, which is comparable to the estimate given by equation (44).

The temperature field given by equation (45) generates gradients in σ and ε, giving rise to an electrical body force. Using the analytical expression for the electric field for the two co-planar electrodes, $\boldsymbol{E} = (V/\pi r)\boldsymbol{u}_\theta$, the expression for the volume force is

$$\boldsymbol{f}_E = -M\frac{\varepsilon\sigma V^4}{8k(\pi r)^3 T}\left(1 - \frac{2\theta}{\pi}\right)\boldsymbol{u}_\theta \quad (46)$$

In this expression M is a dimensionless factor given by

$$M = \frac{(T/\sigma)(\partial\sigma/\partial T) - (T/\varepsilon)(\partial\varepsilon/\partial T)}{1 + (\omega\varepsilon/\sigma)^2} + \frac{1}{2}\frac{T}{\varepsilon}\frac{\partial\varepsilon}{\partial T} \quad (47)$$

It predicts the variation of force with frequency (at $T = 300\,\mathrm{K}$ and for $\omega\varepsilon/\sigma \ll 1$, $M = +6.6$; for $\omega\varepsilon/\sigma \gg 1$, $M = -0.6$). An analytical solution for the velocity in the simplified system shown in figure 1 can be obtained by substituting the force given by equation (46) into the expression for velocity, equation (30). This analytical solution assumes that the frequency is high enough for the electrode polarization to be neglected. With this assumption, the potential at the electrodes is fixed and the velocity is zero at the electrodes. The radial component of the velocity varies from zero at $\theta = 0, \pi$ (the electrodes) to a maximum at $\theta = \pi/2$ and is given by

$$v_{\mathrm{max}} = 5.28 \times 10^{-4}\frac{|M|}{T}\frac{\varepsilon\sigma V^4}{k\eta r} \quad (48)$$

The maximum velocity can be estimated for two cases: $\omega\varepsilon/\sigma \ll 1$ and $\omega\varepsilon/\sigma \gg 1$

$$v_{\mathrm{max}}_{\varepsilon\omega/\sigma\ll 1} \sim 5 \times 10^{-4}\frac{\varepsilon\sigma V^4}{k\eta r}\left|\frac{1}{\sigma}\frac{\partial\sigma}{\partial T}\right|$$

$$v_{\mathrm{max}}_{\varepsilon\omega/\sigma\gg 1} \sim 2.5 \times 10^{-4}\frac{\varepsilon\sigma V^4}{k\eta r}\left|\frac{1}{\varepsilon}\frac{\partial\varepsilon}{\partial T}\right| \quad (49)$$

Note that because the electric field varies as $1/r$, the velocity has a singularity at $r = 0$. Calculations of the velocity using the finite element method have been made for the two-finger strip electrode shown in figure 1. Equations (49) agree with the finite element calculations if r is set equal to the value of the typical dimension of the convective roll in the computations. This value lies between the interelectrode gap length ($25\,\mu\mathrm{m}$) and the height of the upper boundary ($200\,\mu\mathrm{m}$).

5.1.2. Buoyancy. The gravitational body force generated by a temperature field, as given in (41), is

$$f_{\mathrm{g}} = \left(\frac{\partial\rho_{\mathrm{m}}}{\partial T}\right)\frac{\sigma V^2}{2k}\left(\frac{\theta}{\pi} - \frac{\theta^2}{\pi^2}\right)g \quad (50)$$

An order of magnitude estimate of the ratio between the electrical and gravitational forces for $\omega\varepsilon/\sigma \ll 1$ gives

$$\frac{f_{\mathrm{g}}}{f_{\mathrm{E}}} \sim \frac{(\partial\rho_{\mathrm{m}}/\partial T)(\pi r)^3 g}{(1/\sigma)(\partial\sigma/\partial T)\varepsilon V^2} \quad (51)$$

For a characteristic length $r = 25\,\mu\mathrm{m}$ and applied voltage $V = 10\,\mathrm{V}$ (with other parameters as for water) the ratio of $f_{\mathrm{g}}/f_{\mathrm{E}} \sim 7 \times 10^{-4}$ showing that the gravitational force is negligible compared to the electrical force. As the characteristic length of the system is increased, the magnitude of the gravitational force becomes greater than the electrical force. The transition is at $r \approx 300\,\mu\mathrm{m}$ for this applied voltage of $V = 10\,\mathrm{V}$. Finite element calculations confirm that a transition between buoyancy and electrical convection is obtained for a characteristic length $r = 300\,\mu\mathrm{m}$. The numerical calculations indicate that a typical velocity magnitude for a buoyancy flow is

$$v_{\mathrm{max}} \sim 2 \times 10^{-2}\left(\frac{\partial\rho_{\mathrm{m}}}{\partial T}\right)\frac{\sigma V^2 g r^2}{k\eta} \quad (52)$$

5.2. External sources of heat

5.2.1. Electrothermal flow. In addition to Joule heating, a temperature gradient can be generated by an external source, giving rise to electrothermal fluid flow. The heat source generates a temperature gradient in the system, which in turn produces electrical body forces, as given by equation (33), and fluid flow occurs.

Considering an imposed vertical gradient of temperature $\nabla T = -\partial T/\partial y|u_y$ and an electric field given by $E = V/\pi r u_\theta$, the electrical body force is

$$f_{\mathrm{E}} \approx \frac{1}{2}\varepsilon\left(\frac{V}{\pi r}\right)^2\left|\frac{\partial T}{\partial y}\right|\left|\frac{1}{\sigma}\frac{\partial\sigma}{\partial T}\right|\cos\theta\,u_\theta$$

$$\text{for } \omega \ll \sigma/\varepsilon$$

$$(53a)$$

and

$$f_{\mathrm{E}} = -\frac{1}{4}\varepsilon\left(\frac{V}{\pi r}\right)^2\left|\frac{\partial T}{\partial y}\right|\left|\frac{1}{\varepsilon}\frac{\partial\varepsilon}{\partial T}\right|(\cos\theta\,u_\theta + \sin\theta\,u_r)$$

$$\text{for } \omega \gg \frac{\sigma}{\varepsilon}$$

$$(53b)$$

For saline solutions, the frequency at which the behaviour changes is given by

$$\omega \sim \frac{\sigma}{\varepsilon}\left|\frac{(1/\sigma)(\partial\sigma/\partial T)}{(1/\varepsilon)(\partial\varepsilon/\partial T)}\right|^{1/2} \sim 2\frac{\sigma}{\varepsilon} \quad (54)$$

The ratio between the amplitudes of the velocity at the high and low frequency limits is

$$\frac{v_{\mathrm{low}}}{v_{\mathrm{high}}} \sim \frac{f_{\mathrm{low}}}{f_{\mathrm{high}}} \sim \frac{|(1/\sigma)(\partial\sigma/\partial T)|}{|(1/\varepsilon)(\partial\varepsilon/\partial T)|} \sim 5 \quad (55)$$

According to the Stokes equation, the fluid velocity should scale as $v \propto f_{\mathrm{E}}r^2/\eta$. Numerical calculations using finite element methods [11] indicate that the maximum value for the velocity generated in the fluid (when $\omega \ll \sigma/\varepsilon$) is

$$v_{\mathrm{max}} \sim 3 \times 10^{-3}\frac{\varepsilon V^2}{\eta}\left|\frac{\partial T}{\partial y}\right|\left|\frac{1}{\sigma}\frac{\partial\sigma}{\partial T}\right| \quad (56)$$

A possible external heat source is the incident light that is used for the observation of the micro-devices under strong illumination [10]. Both experiment and calculations [10, 11] suggest that there is a vertical gradient in temperature, with the electrodes at a temperature above room temperature. Expressions (54) and (55) have been confirmed by experiment [10]. The calculations [11] agree with observations [10] if an imposed vertical temperature gradient of $0.021\,\mathrm{K}\,\mu\mathrm{m}^{-1}$ is assumed. According to equation (56), the fluid velocity is independent of the size of the system for any externally imposed vertical temperature gradient. In the experimental work on light-induced flow [10], it was assumed that a given fraction of the light power is transformed to heat at the electrodes. If the light power per unit area is kept constant, but the size of the system is changed, the heat flux will remain constant, as will the vertical gradient of temperature, since $Q = -k\partial T/\partial y$.

5.2.2. Buoyancy. The gravitational body force generated by a vertical gradient in temperature can be compensated by a pure pressure gradient, so that there is no fluid motion. The Rayleigh–Benard instability breaks this equilibrium at

sufficiently high temperature gradients. If Rayleigh's number is of the order of 1500, natural convection can take place, i.e.

$$\text{Ra} = \frac{g|\partial\rho_m/\partial T|\Delta T h^3}{\eta\chi} \sim 1500 \tag{57}$$

where χ is the thermal diffusivity coefficient and h a system height. For an increment of temperature $\Delta T \sim 10\,\text{K}$, a typical system height of 2 mm would be required to demonstrate the instability.

5.3. AC electro-osmosis

Recent work has shown that the application of an ac voltage to a pair of co-planar microelectrodes generates a steady (non-zero time-averaged) fluid flow with a velocity that depends both on the applied potential and frequency [5, 6]. A simple circuit model based on an array of resistors and capacitors gives reasonable correlation with experimentally observed values of velocity. This model consists of semicircular resistors connecting one electrode to the other, terminated at either end on the electrodes by a capacitor representing the electrical double layer [5]. This model can be refined by taking into account the full linear electrokinetic equations for the double layer and the electrolyte [7]. Significantly, the results of such an analysis are in good agreement with the simpler resistor–capacitor model. According to equation (42), the potential drop across the double layer $\Delta\phi_{\text{DL}}$ must be estimated. Using simple circuit theory, $\Delta\phi_{\text{DL}}$ is

$$\Delta\phi_{\text{DL}} = \frac{V/2}{1 + i\pi C\omega r/2\sigma} \tag{58}$$

and the slip velocity is

$$v_{\text{slip}} = \Lambda \frac{\varepsilon V^2}{8\eta r} \frac{\Omega^2}{(1+\Omega^2)^2} \tag{59}$$

with a non-dimensional frequency Ω given by

$$\Omega = \frac{\omega C\pi r}{2\sigma} \tag{60}$$

The capacitance C is given by ΛC_D, with $C_D = \varepsilon/\lambda_D$, the surface capacitance of the diffuse double layer in the Debye–Huckel model. The electrodes used to characterize fluid flow were made of titanium and have a thin surface oxide. For a suspending medium conductivity of $2.1 \times 10^{-3}\,\text{S m}^{-1}$, and using titanium electrodes, Λ was found by experiment to be ≈ 0.25. This indicates that the potential drop across the diffuse part of the double layer is only a quarter of the potential drop across the entire double layer. For an ideal double layer consisting of a Stern layer and a diffuse layer, the parameter Λ decreases with conductivity, since $\Lambda = C_S/(C_S + C_D)$ where C_D, the capacitance of the diffuse layer, increases with conductivity. Experimentally, the value of the Stern layer capacitance must be set equal to $C_S \sim 0.007\,\text{F m}^{-2}$ for agreement with the experimentally determined value of Λ [6, 8]. Expression (56) for the velocity comes from the application of linear theory (small voltages) and the assumption of perfectly polarizable electrodes. Experiments show that this expression is a fair representation of the velocity, even for the non-linear case and for non-ideal double layers.

The frequency dependence of the fluid velocity shows a broad maximum, tending to zero as the frequency goes to zero or infinity. The maximum velocity is obtained at $\Omega = 1$, i.e. for an angular frequency $\omega_0 = 2\sigma/(C\pi r)$. Taking $C_D = \varepsilon/\lambda_D$, the angular frequency where maximum fluid velocity occurs is $\omega_0 = 2\sigma\lambda_D/\varepsilon\pi r\Lambda$. This is several orders of magnitude smaller than the charge relaxation frequency of the liquid $\omega = \sigma/\varepsilon$. For frequencies much smaller than ω_0 the applied voltage is dropped mainly across the double layer; the electric field outside the double layer becomes very small. For frequencies much greater than ω_0, the applied voltage is dropped mainly across the electrolyte and the surface charge accumulated in the double layer is very small. In both cases, the electro-osmotic slip velocity is very small, cf equation (59).

6. Results and discussion: scaling laws

In section 2 it was shown that a particle has a terminal velocity given by $\boldsymbol{u} = \boldsymbol{v} + \boldsymbol{F}/\gamma$, where $\boldsymbol{v}$ is the fluid velocity (which may be the sum of different flows because the equations are linear) and $\boldsymbol{F}/\gamma$ the velocity induced on the particle by the different forces acting upon it. The random displacement of Brownian motion must be added to the displacement of the particle. Table 2 summarises the equations, giving order of magnitude estimates of displacements in a given time t for a particle moving above a micro-electrode, such as that shown in figure 1.

At low frequencies (Ω of order one or smaller), polarization of the double layer can significantly reduce the voltage present in the electrolyte. From simple circuit analysis, the voltage across the electrolyte is $V - 2\Delta\phi_{\text{DL}}$, where $\Delta\phi_{\text{DL}}$ is given by equation (58), so that the voltage amplitude in

Table 2. Estimated displacements for a particle (latex sphere) in the simplified microelectrode structure shown in figure 1. From experiments (in [6, 8]) a value of $C_S \sim 0.007\,\text{F m}^{-2}$ has been used. The factor c takes into account the reduction of the voltage in the medium due to electrode polarization and is given by $\Omega/\sqrt{1+\Omega^2}$.

Gravity	$0.2\dfrac{a^2\rho_m g}{\eta}t$
Dielectrophoresis	$0.03\dfrac{a^2\varepsilon}{\eta}\dfrac{(cV)^2}{r^3}t$
Brownian displacement	$\sqrt{\dfrac{k_B T t}{3\pi a\eta}}$
Electrothermal ($\varepsilon\omega/\sigma \ll 1$)	$5\times 10^{-4}\dfrac{\varepsilon\sigma(cV)^4}{k\eta r}\left|\dfrac{1}{\sigma}\dfrac{\partial\sigma}{\partial T}\right|t$
Electrothermal ($\varepsilon\omega/\sigma \ll 1$)	$2.5\times 10^{-4}\dfrac{\varepsilon\sigma(cV)^4}{k\eta r}\left|\dfrac{1}{\varepsilon}\dfrac{\partial\varepsilon}{\partial T}\right|t$
Buoyancy	$2\times 10^{-2}\left(\dfrac{\partial\rho_m}{\partial T}\right)\dfrac{\sigma(cV)^2 gr^2}{k\eta}t$
Light-electrothermal ($\varepsilon\omega/\sigma \ll 1$)	$3\times 10^{-3}\dfrac{\varepsilon(cV)^2}{\eta}\left|\dfrac{\partial T}{\partial y}\right|\left|\dfrac{1}{\sigma}\dfrac{\partial\sigma}{\partial T}\right|t$
AC electro-osmosis	$0.1\,\Lambda\dfrac{\varepsilon V^2}{\eta r}\dfrac{\Omega^2}{(1+\Omega^2)^2}t,$ $\Omega = \Lambda\dfrac{\omega\varepsilon\pi r}{2\sigma\lambda_D},$ $\Lambda = \dfrac{C_S}{(C_S + C_D)}$

the electrolyte is $V\Omega/\sqrt{1+\Omega^2}$. In other words, at low frequencies, the voltage in the electrolyte is reduced by a factor of the order of $c = \Omega\sqrt{1+\Omega^2}$, where the parameter c is used to scale the applied potential V when calculating bulk fluid flow (sections 5.1 and 5.2) and dielectrophoretic displacement at low frequencies.

6.1. Fluid flow

In this section, comparisons of the relative magnitudes of the different flow velocities are made. Except where otherwise indicated, external sources of heat are assumed to be absent. Figures 5 and 6 show iso-lines of fluid velocity plotted for different applied voltages V and characteristic system lengths r. The iso-lines are calculated fluid velocities generated by the dominant mechanism, either Joule-heating

(electrothermal and buoyancy) or ac electro-osmosis. Velocity contours below 10^{-8} m s^{-1} are considered insignificant for characteristic system lengths greater than 10^{-6} m and are ignored (white region in the diagrams). A typical case for a low conducting electrolyte ($\sigma = 10^{-3}$ S m^{-1}) is shown in figure 5; comparison with a high conducting electrolyte ($\sigma = 10^{-1}$ S m^{-1}) is made in figure 6. Low frequency behaviour is plotted in figure 5(a) ($f = 0.1$ kHz) and figure 6(a) ($f = 10$ kHz); high frequencies in figure 5(b) ($f = 0.1$ MHz) and figure 6(b) ($f = 10$ MHz). Low frequencies are defined as frequencies much lower than the charge relaxation frequency ($\omega\varepsilon/\sigma = 4.4 \times 10^{-4}$); high frequencies correspond to a frequency of the order of the charge relaxation frequency ($\omega\varepsilon/\sigma = 0.44$) and above.

Before interpreting the maps, it should be noted that certain regions are inaccessible; electrolysis at the electrode surface occurs at low frequencies and high voltages, and
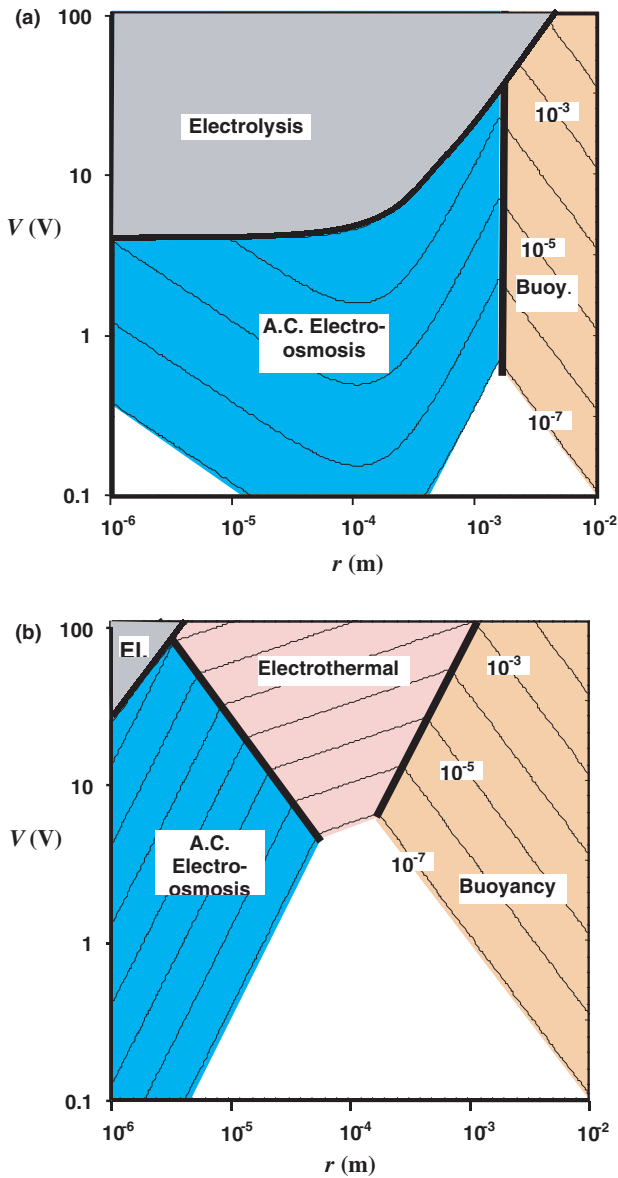

Figure 5. Fluid flow map in the plane V versus r for a medium with $\sigma = 10^{-3}$ S m^{-1}: (a) $f = 10^2$ Hz ($\omega\varepsilon/\sigma = 4.4 \times 10^{-4}$); (b) $f = 10^5$ Hz ($\omega\varepsilon/\sigma = 0.44$). Note that the velocity contours are in units of m s^{-1}.
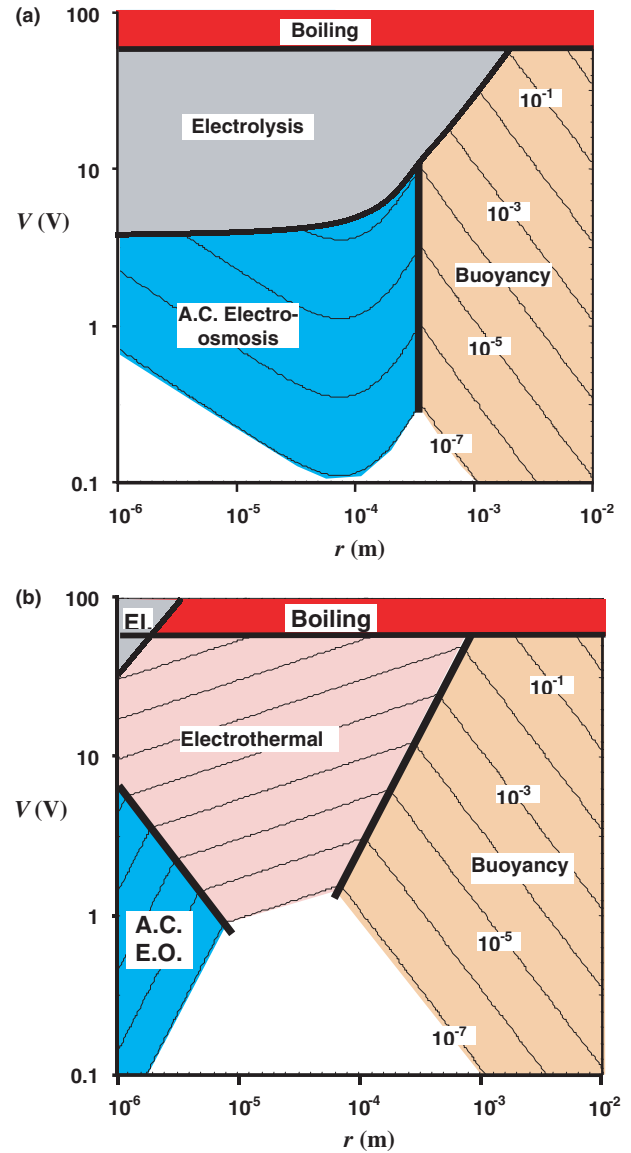
Figure 6. Fluid flow map in the plane V versus r for a medium with $\sigma = 10^{-1}$ S m^{-1}: (a) $f = 10^4$ Hz ($\omega\varepsilon/\sigma = 4.4 \times 10^{-4}$); (b) $f = 10^7$ Hz ($\omega\varepsilon/\sigma = 0.44$). The velocity contours are in units of m s^{-1}.

boiling due to Joule heating occurs at high voltages and conductivities. Under dc conditions, a few volts are enough to produce electrolysis [20]; assuming that 2 V across the double layer is needed to produce electrolysis ($|\Delta\phi_{DL}| = 2$ V), the maximum permissible applied voltage is given by $V = 4\sqrt{1 + \Omega^2}$ V. According to equation (45), the maximum applied voltage before boiling takes place is given by $V = \sqrt{8k\Delta T/\sigma}$, where $\Delta T \sim 75$ K (for a room temperature of 25°C). These boundaries are also depicted in the maps.

As is apparent from the figures, ac electro-osmosis progressively disappears when the frequency is increased. It dominates at low frequencies, and small characteristic lengths, and can reach velocities of several mm s^{-1}. As the electrolyte conductivity is increased, the effect of electrothermal flow becomes more important. At a characteristic system length of the order of 1 mm, buoyancy due to Joule heating always dominates the fluid flow.

The experimental observations of ac electro-osmosis [6, 8, 21] confirm that it can dominate the behaviour of particles at low frequencies, as suggested by figures 5(*a*) and 6(*a*). Note that the effect decreases with increasing conductivity. Electrothermal travelling wave pumping experiments [4, 22] show that voltages greater than 10 V are required to achieve noticeable fluid velocities, in agreement with the calculated voltages shown in the figures. The velocity measurements given in [22] show that strong thermal convection is obtained for conductivities greater than 1.6×10^{-2} S m^{-1}. In the same work, it was shown that the velocity increases with conductivity (in the measured range of 4×10^{-3} to 1.6×10^{-2} S m^{-1}), which is a clear indication of Joule heating. However, in this same set of experiments, no noticeable dependence of flow velocity on conductivity was observed for conductivities lower than 4×10^{-3} S m^{-1}; the reason for this is not clear. In another set of experiments [23, 24], it has been reported that the time-dependent collection of particles in a millimetre-scale system can be driven by Joule heating-induced buoyancy forces. Large convective rolls were observed, with typical dimensions and velocities in agreement with the characteristic system length and expected flow velocity shown in the maps.

Figure 7 shows the domain of influence of Joule heating and light-induced electrothermal flow, plotted as a function of voltage and conductivity. A characteristic system length of $r = 50\,\mu$m has been chosen. For the light-induced heating, two vertical gradients of temperature are used: 0.02 K μm^{-1} in figure 7(*a*) and 0.002 K μm^{-1} in figure 7(*b*). The former temperature gradient corresponds to that which was required to numerically model experimentally observed fluid velocities under strong illumination [11] (at a conductivity of 2.1×10^{-3} S m^{-1}). The variation in flow with conductivity is very small since $(1/\sigma)(d\sigma/dT)$ is almost independent of conductivity. Figure 7(*a*) shows that only for very high applied voltages and conductivities is Joule heating more important than the externally imposed temperature gradient of 0.02 K μm^{-1}. If the temperature gradient is reduced by a factor of 10 (figure 7(*b*)), light-induced fluid flow still occurs for conductivities smaller than 10^{-2} S m^{-1} and applied voltages below 10 V, but the expected velocities are ten times smaller.
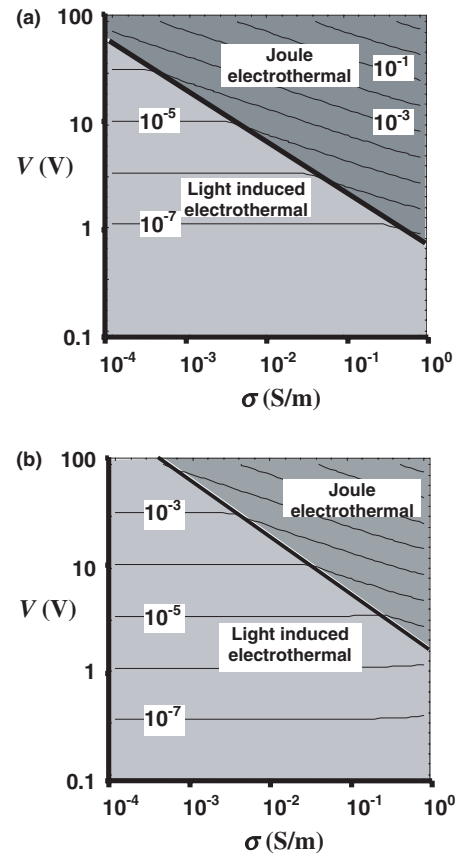
Figure 7. Fluid flow map showing joule heating and light-induced heating electrothermal flows in the plane V versus σ. (*a*) $dT/dy = 0.02$ K μm^{-1}; (*b*) $dT/dy = 0.002$ K μm^{-1}. The velocity contours are in units of m s^{-1}.

6.2. Particle displacement

Figure 8 shows the displacement of a particle for a time window of 1 s in an electrolyte with conductivity 10^{-2} S m^{-1}, plotted as a function of particle radius (with the same parameters as used to plot figure 3). The first point to note is that ac electro-osmosis dominates particle motion at a frequency of 1 kHz. Only for large particles (greater than 5 μm in diameter) is the ac electro-osmotic-induced displacement less than that caused by DEP. This concurs with experimental observations, particularly of cells, where the subtle effects of ac electro-osmosis on particle dynamics at low frequencies are often unnoticed. The electro-osmotic displacement becomes negligible at high frequencies, as shown by the line calculated at $f = 1$ MHz. This diagram shows that movement of sub-micron sized particles by DEP at low frequencies ($\sim$1 kHz) is almost impossible owing to ac electro-osmosis. At frequencies around 1 MHz, ac electro-osmosis is irrelevant and DEP dominates. However, as the particle size is decreased, the voltage required to induce particle movement becomes appreciably greater. This means that electrothermal flow due to Joule heating can become important.

The data can be plotted in a different way; figure 9 shows the displacement of a small particle (0.5 μm diameter) as a function of voltage for a small electrode structure (characteristic length $r = 25\,\mu$m). Again, displacement due to electro-osmosis dominates at low frequencies ($\sim$1 kHz) but
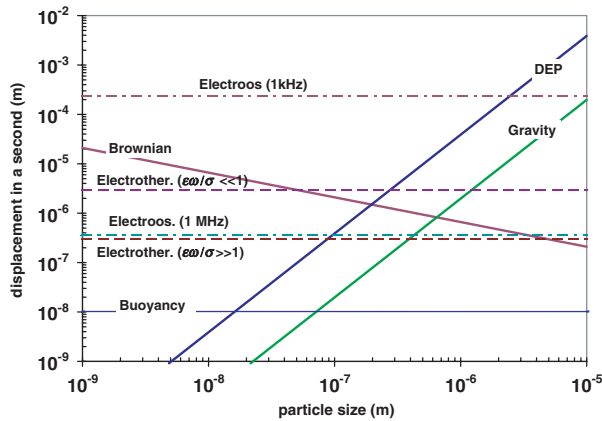
Figure 8. Particle displacement in 1 s versus particle radius ($V = 5\,\mathrm{V}$, $r = 25\,\mu\mathrm{m}$, $\sigma = 0.01\,\mathrm{S\,m^{-1}}$).

Figure 10. Particle displacement in 1 s versus characteristic length ($a = 0.25\,\mu\mathrm{m}$, $V = 5\,\mathrm{V}$, $\sigma = 0.01\,\mathrm{S\,m^{-1}}$).

Figure 9. Particle displacement in 1 s versus applied voltage ($a = 0.25\,\mu\mathrm{m}$, $r = 25\,\mu\mathrm{m}$, $\sigma = 0.01\,\mathrm{S\,m^{-1}}$).

is negligible at high frequencies (1 MHz) compared to DEP. In order to overcome Brownian random displacement and produce deterministic motion of small particles, the voltage must be increased. However, the electrothermal effect due to Joule heating becomes clearly dominant over DEP for voltages greater than 10 V. In figure 9, the electrothermal displacement is plotted for frequencies corresponding to $\omega \ll \sigma/\varepsilon$. If the frequency is increased so that $\omega \gg \sigma/\varepsilon$, the electrothermal effect is reduced by up to a factor of 10. In an experiment, the characteristic length of a fluid roll could be greater than the characteristic length for DEP (here chosen to be $25\,\mu\mathrm{m}$) so that the expected electrothermal displacement would in fact be smaller than that shown on the graph.

The effect of changing the characteristic length of the system can be seen in figure 10. As this increases, the electrothermal, electro-osmotic and DEP effects all decrease. At a characteristic length close to 1 mm, buoyancy due to Joule heating becomes important. This produces large fluid rolls and slow particle motion, as observed experimentally [23, 24]. The DEP motion is clearly dominant at small scales. In this case, the characteristic length r can be thought of as the distance to the electrode edge, showing that particles are easily trapped at those points by positive DEP, i.e. positive DEP can trap particles at electrode edges while they are moved by fluid motion in the bulk [2, 25].
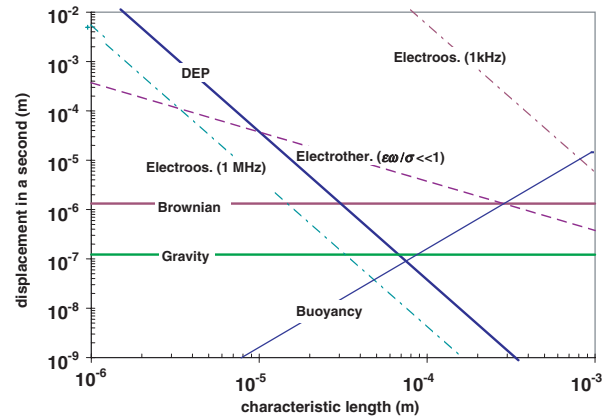
To illustrate the domains of influence of the different forces (Brownian, DEP, ac electro-osmosis, electrothermal and buoyancy) acting on a sub-micron particle, the iso-lines of displacement per second due to the dominant mechanism in the plane V versus r are shown in figure 11, for a particle of radius $0.25\,\mu\mathrm{m}$. The Brownian (random) displacement for this particle in 1 s is around $1\,\mu\mathrm{m}$. Deterministic displacements smaller than $1\,\mu\mathrm{m}$ are very difficult to determine for an isolated particle and are plotted as the Brownian region in the maps. Notice that increasing the time of observation or the number of observed particles would allow us to measure velocities smaller than $1\,\mu\mathrm{m\,s^{-1}}$. Figure 11 shows these maps for a particle in a low conducting electrolyte, $\sigma = 10^{-3}\,\mathrm{S\,m^{-1}}$; figure 11(a) for low frequencies (0.1 kHz), and figure 11(b) for high frequencies (0.1 MHz). It is evident from the figure that DEP is overriden by ac electro-osmosis at low frequencies for small system sizes (small r). Figure 12 shows the corresponding domains of influence for the same particle in a high conducting electrolyte, $\sigma = 0.1\,\mathrm{S\,m^{-1}}$, for low (10 kHz) and high frequencies (10 MHz). At low frequencies and for small system sizes ($<1\,\mathrm{mm}$) either ac electro-osmosis dominates (although with smaller velocity amplitude than in figure 11(a)) or the voltage is high enough to produce electrolysis. For small systems and high frequencies, DEP is again the dominant effect. For high frequencies, electrothermal dominates at high voltages and moderate systems and buoyancy dominates for moderate voltages and large systems. For both electrothermal and buoyancy effects, the domains of influence increase with conductivity (compare figures 11(b) and 12(b)). Care should be taken to avoid boiling at high voltages ($\sim 75\,\mathrm{V}$).

7. Conclusions and summary

The movement of liquid and the behaviour of particles in aqueous solutions subjected to ac electric fields has been examined. The high strength electric fields used in DEP separation systems often give rise to fluid motion, which in turn results in a viscous drag on the particle. This fluid flow occurs because electric fields generate heat, leading to volume forces in the liquid. Gradients in conductivity and permittivity give rise to electrothermal forces and gradients in
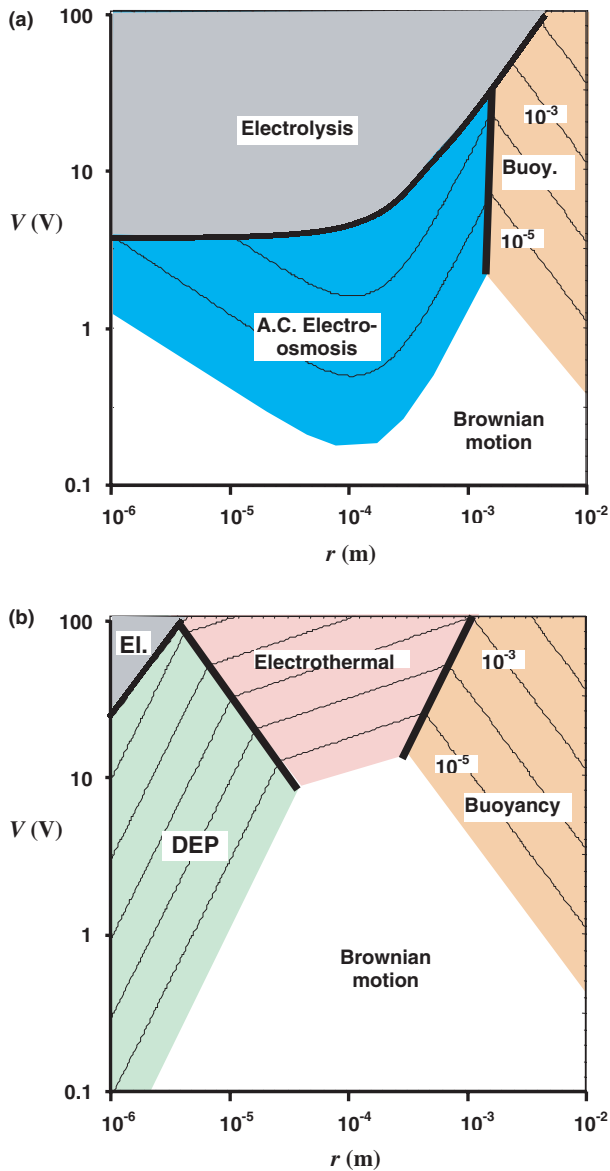
Figure 11. Particle velocity maps in the plane V versus r for a particle with radius $a = 0.25\,\mu$m in medium with $\sigma = 10^{-3}\,\mathrm{S\,m^{-1}}$: (*a*) $f = 10^2$ Hz; (*b*) $f = 10^5$ Hz.

Figure 12. Particle velocity maps in the plane V versus r for a particle with radius $a = 0.25\,\mu$m in medium with $\sigma = 0.1\,\mathrm{S\,m^{-1}}$: (*a*) $f = 10^4$ Hz; (*b*) $f = 10^7$ Hz.

mass density to buoyancy. In addition, non-uniform ac electric fields produce forces on the induced charges in the diffuse double layer on the electrodes. This effect gives oscillating and steady fluid motions termed ac electro-osmosis. We have focused on steady fluid flow. The effects of Brownian motion have also been discussed in this context. The orders of magnitude of the various forces experienced by a particle in a model microelectrode system have been estimated. The results indicate that ac electro-osmosis dominates fluid motion at low frequencies and small system sizes, electrothermal flow dominates at high frequencies and voltages, and buoyancy at typical system sizes of the order of or greater than 1 mm. DEP governs the motion of sub-micrometre particles for small systems and at high frequencies; otherwise, the particle motion is due to fluid drag as shown in figures 11 and 12.
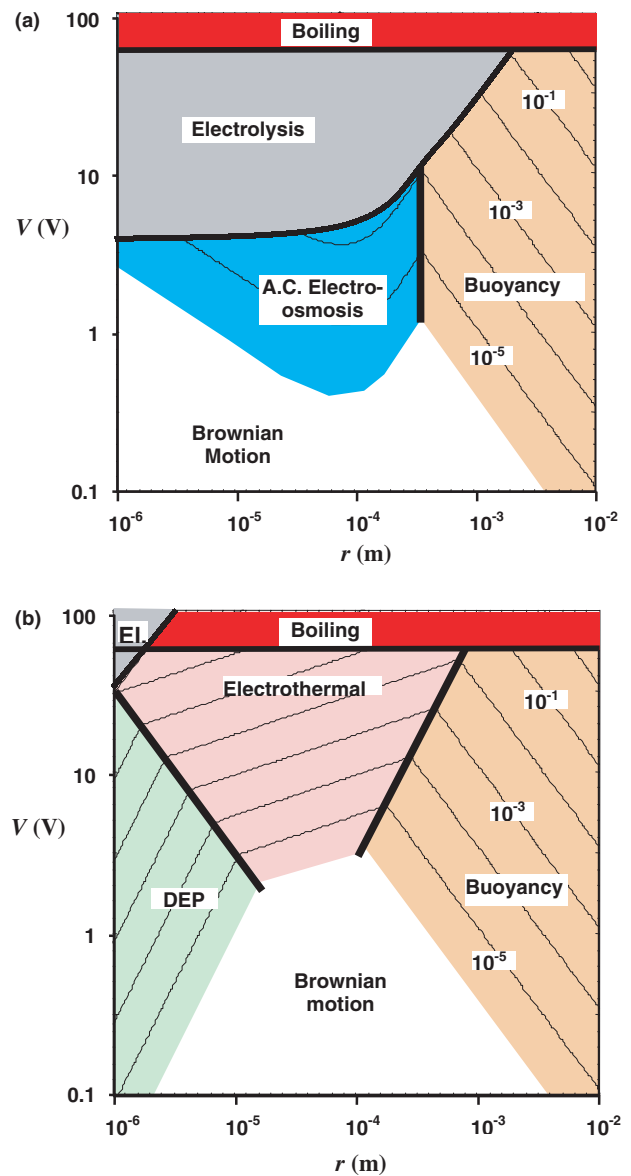
References

[1] Morgan H and Green N G 2003 *AC Electrokinetics: Colloids and Nanoparticles* (Herts: Research Studies Press)
[2] Muller T, Gerardino A, Schnelle T, Shirley S G, Bordoni F, DeGasperis G, Leoni R and Fuhr G 1996 Trapping of micrometre and sub-micrometre particles by high-frequency electric fields and hydrodynamic forces *J. Phys. D: Appl. Phys.* **29** 340–9
[3] Ramos A, Morgan H, Green N G and Castellanos A 1998 AC electrokinetics: a review of forces in microelectrode structures *J. Phys. D: Appl. Phys.* **31** 2338–53
[4] Fuhr G, Hagedorn R, Müller T, Benecke W and Wagner B 1992 Microfabricated electrohydrodynamic (EHD) pumps for liquids of higher conductivity *J. Microelectromech. Syst.* **1** 141–6
[5] Ramos A, Morgan H, Green N G and Castellanos A 1999 AC electric-field induced fluid flow in microelectrodes *J. Colloid Interface Sci.* **217** 420–2

[6] Green N G, Ramos A, Gonzalez A, Morgan H and Castellanos A 2000 Fluid flow induced by non-uniform ac electric fields in electrolytes on microelectrodes I: experimental measurements *Phys. Rev.* E **61** 4011–18

[7] González A, Ramos A, Green N G, Castellanos A and Morgan H 2000 Fluid flow induced by non-uniform ac electric fields in electrolytes on microelectrodes II: A linear double-layer analysis *Phys. Rev.* E **61** 4019–28

[8] Green N G, Ramos A, González A, Morgan H and Castellanos A 2002 Fluid flow induced by non-uniform ac electric fields in electrolytes on microelectrodes III: Observation of streamlines and numerical simulation *Phys. Rev.* E **66** 026305

[9] Reppert P M and Morgan F D 2002 Frequency-dependent electroosmosis *J Colloid Interface Sci.* **254** 372–83

[10] Green N G, Ramos A, González A, Castellanos A and Morgan H 2000 Electric field induced fluid flow on microelectrodes: the effect of illumination *J. Phys. D: Appl. Phys.* **33** L13–17

[11] Green N G, Ramos A, Morgan H, Castellanos A and González A 2001 Electrothermally induced fluid flow on microelectrodes *J. Electrost.* **53** 71–87

[12] Clift R, Grace J R and Weber M E 1978 *Bubbles, Drops and Particles* (New York: Academic) chapter 11

[13] Green N G, Ramos A and Morgan H 2000 AC electrokinetics: a survey of sub-micrometre particle dynamics *J. Phys. D: Appl. Phys.* **33** 632–41

[14] Castellanos A (ed) 1998 *Electrohydrodynamics* (New York: Springer)

[15] Saville D A 1997 Electrohydrodynamics: the Taylor-Melcher leaky dielectric model *Ann. Rev. Fluid Mech.* **29** 27–64

[16] Melcher J R and Taylor G I 1969 Electrohydrodynamics: a review of the role of interfacial shear stresses *Ann. Rev. Fluid Mech.* **1** 111–46

[17] Batchelor G K 1967 *An Introduction to Fluid Dynamics* (Cambridge: Cambridge University Press)

[18] Stratton J A 1941 *Electromagnetic Theory* (New York: McGraw-Hill)

[19] Hunter R J 1981 *Zeta Potential in Colloid Science* (London: Academic)

[20] Hamann C H, Hamnett A and Vielstich W 1998 *Electrochemistry* (Weinheim: Wiley-VCH)

[21] Brown A B D, Smith C G and Rennie A R 2001 Pumping of water with ac electric fields applied to asymmetric pairs of microelectrodes *Phys. Rev.* E **63** 016305

[22] Gimsa J, Eppmann P and Pruger B 1997 Introducing phase analysis light scattering for dielectric characterization: measurement of travelling-wave pumping *Biophys. J.* **73** 3309–16

[23] Arnold W M and Chapman B 2002 The Lev-vection particle concentrator: some operational characteristics *IEEE Conf. Elec. Ins. Dielectric Phenomena*

[24] Arnold W M 2001 Positioning and levitation media for the separation of biological cells *IEEE Trans. Ind. Appl.* **37** 1468–75

[25] Green N G and Morgan H 1998 Separation of submicrometre particles using a combination of dielectrophoresis and electrohydrodynamic forces *J. Phys. D: Appl. Phys.* **31** L25–30